AGU PUBLICATIONS

Geophysical Research Letters

RESEARCH LETTER
10.1002/2015GL067336

Key Point:
- Geodetic and seismic observations require millenary $M_w > 9.0$ earthquakes along the Himalaya

Supporting Information:
- Supporting Information S1

Correspondence to:
V. L. Stevens,
vstevens@caltech.edu

Citation:
Stevens, V. L., and J.-P. Avouac (2016), Millenary $M_w > 9.0$ earthquakes required by geodetic strain in the Himalaya, *Geophys. Res. Lett.*, *43*, 1118–1123, doi:10.1002/2015GL067336.

Received 8 DEC 2015
Accepted 15 JAN 2016
Accepted article online 22 JAN 2016
Published online 13 FEB 2016

Millenary $M_w > 9.0$ earthquakes required by geodetic strain in the Himalaya

V. L. Stevens[1] and J.-P. Avouac[1]

[1]California Institute of Technology, Pasadena, California, USA

Abstract The Himalayan arc produced the largest known continental earthquake, the $M_w \approx 8.7$ Assam earthquake of 1950, but how frequently and where else in the Himalaya such large-magnitude earthquakes occur is not known. Paleoseismic evidence for coseismic ruptures at the front of the Himalaya with 15 to 30 m of slip suggests even larger events in medieval times, but this inference is debated. Here we estimate the frequency and magnitude of the largest earthquake in the Himalaya needed so that the moment released by seismicity balances the deficit of moment derived from measurements of geodetic strain. Assuming one third of the moment buildup is released aseismically and the earthquakes roughly follow a Gutenberg-Richter distribution, we find that $M_w > 9.0$ events are needed with a confidence level of at least 60% and must return approximately once per 800 years on average.

1. Introduction

Subduction megathrust faults are known to produce the largest earthquakes on Earth, which can reach a moment magnitude (M_w) well above 9.0. Whether continental megathrust faults, such as the Main Himalayan Thrust (MHT) along which the Himalayan wedge is thrust over India, can host such large earthquakes is less clear. Geodetic measurements of interseismic strain indicate that the MHT is nearly completely locked over a ~120 km width all along the arc [*Ader et al.*, 2012; *Bilham et al.*, 1997; *Mukul et al.*, 2010; *Schiffman et al.*, 2013; *Stevens and Avouac*, 2015] (Figure 1a). Locking results in a moment deficit accumulating at a rate of $15.1 \pm 1.1 \times 10^{19}$ Nm/yr. The interseismic locking pattern is probably stationary as indicated from the correlation with topography. The 3500 m elevation contour line outlines the downdip edge of the locked fault zone (Figure 1b) and also bounds the northern extent of thrust earthquakes [*Avouac*, 2003; *Bollinger et al.*, 2004]. The along-strike uniform locking, despite different segments being in different stages of the seismic cycle, also suggests that temporal variations are small.

The consistency of geological slip rates with geodetic shortening rates [*Stevens and Avouac*, 2015] requires that transient slip events on the locked portion of the MHT must add up to compensate interseismic slip deficit. This is observed in eastern Nepal where trenches have revealed five to seven >12 m slip events over the last 3600 years, most probably associated with large earthquakes including an M_w8.4 in 1934 and a similar earthquake in 1255 [*Bollinger et al.*, 2014]. The slip budget seems to close locally over this time period [*Bollinger et al.*, 2014]. Paleoseismic studies have revealed even larger (>15 m) slip events around 1100 A.D. at distant sites [*Kumar et al.*, 2010; *Lavé et al.*, 2005; *Upreti et al.*, 2000]. Assuming they are due to the same earthquake, the rupture length would have exceeded 700 km, about twice as long as in 1934. Similarly, a very large earthquake may have ruptured the Himalayan front around 1400 A.D. in the Kumaon-Garwal Himalaya [*Kumar et al.*, 2006] (Figure 1a). Large seismic slip events are documented also in Bhutan [*Berthet et al.*, 2014], although this area is devoid of significant recorded large earthquakes. Paleoseismic studies thus raise the possibility of $M_w > 9.0$ earthquakes.

We confirm Bilham, Gaur, and Molnar's [*Bilham et al.*, 2001] inference that the moment deficit accumulating in the interseismic period outweighs the moment released by the known seismicity. $M_w < 5.5$ earthquakes from local monitoring in the interseismic period release <1% of the moment deficit due to locking of the MHT (Figure 2a). $M_w \leq 7.8$ earthquakes reported in the National Earthquake Information Center (NEIC) catalog (http://neic.usgs.gov) released less than 10% of the interseismic moment deficit over the past 30 years covered by this catalog. Historical earthquakes (Tables S1 and S2 in the supporting information), which reach to M_w8.7, still fall short of balancing interseismic locking. Even if we extend the catalog up to M_w9.0 events to account for the paleoseismic evidence, seismic slip still falls short of balancing the interseismic deficit of slip, as shown from the gap between the seismic moment buildup and release rate from earthquakes

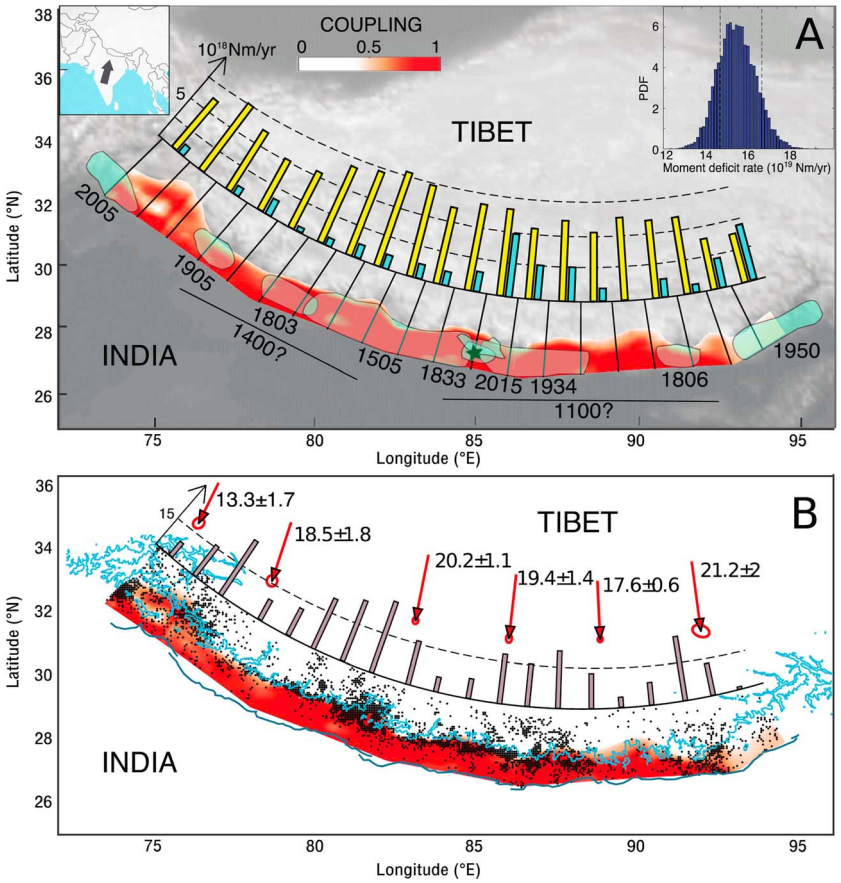

Figure 1. Interseismic coupling and moment buildup on the Main Himalayan Thrust. (a) The pattern of coupling [*Stevens and Avouac*, 2015] is shown in red, overlain by the rough locations of earthquakes M_w7.5–8 for the past 200 years and ≥8 for the past 500 years (4), [*Galetzka et al.*, 2015], which are used in calculating the rate of seismic moment release (light blue bars). The approximate extent of surface ruptures of two potential major earthquakes, dated to ~1400 A.D. and ~1100 A.D. from paleoseismic studies, is also shown. The probability distribution function (pdf) in the inset shows the seismic moment buildup calculated from the coupling model, and the yellow bars show its distribution along the strike of the arc. (b) Same coupling pattern, now with the surface trace of the Main Frontal Thrust [*Styron et al.*, 2011] in dark blue and the 3500 m elevation contour line in light blue. The 3500 m contour seems to mark the downdip extent of the locked fault zone. The MHT appears locked from the surface, where is emerges along the front of the sub-Himalaya, following the trace of the Main Frontal Thrust to beneath the front of the high Himalaya. Red arrows show convergence across the range in mm/yr (7). Black dots show seismicity from the National Seismic Centre (NSC) and NEIC catalogs [*Ader et al.*, 2012; *Stevens and Avouac*, 2015]. The grey bars show the distribution of the number of earthquakes above 4.9 (the magnitude of completeness) of the declustered NEIC catalog (see supporting information for details).

(Figure 2a). The imbalance can also been seen from the comparison of moment release to buildup through time over the past 1000 years (Figure S5).

Balancing the slip budget seems to require more frequent M_w9.0 events than we assumed (1 in 1000 years) or even larger earthquakes. This analysis ignores the role of aseismic slip and the moment accounted for by undetected earthquakes. These factors need to be taken into account to assess quantitatively the slip budget balance and the probability of large events. We first describe the method used and then go on to discuss the results.

2. Method and Data

We assess the magnitude and return period of the largest earthquake needed to balance the slip budget at the scale of the whole Himalayan arc. We assume that fault slip above the brittle-ductile transition, as indicated by the depth distribution of earthquakes, is entirely seismic and that the seismic slip events must add up to match the long-term slip rate on the fault [*Brune*, 1968; *Molnar*, 1979]. We include the contribution of aftershocks and transient aseismic slip in the slip budget. This approach has been applied recently to the

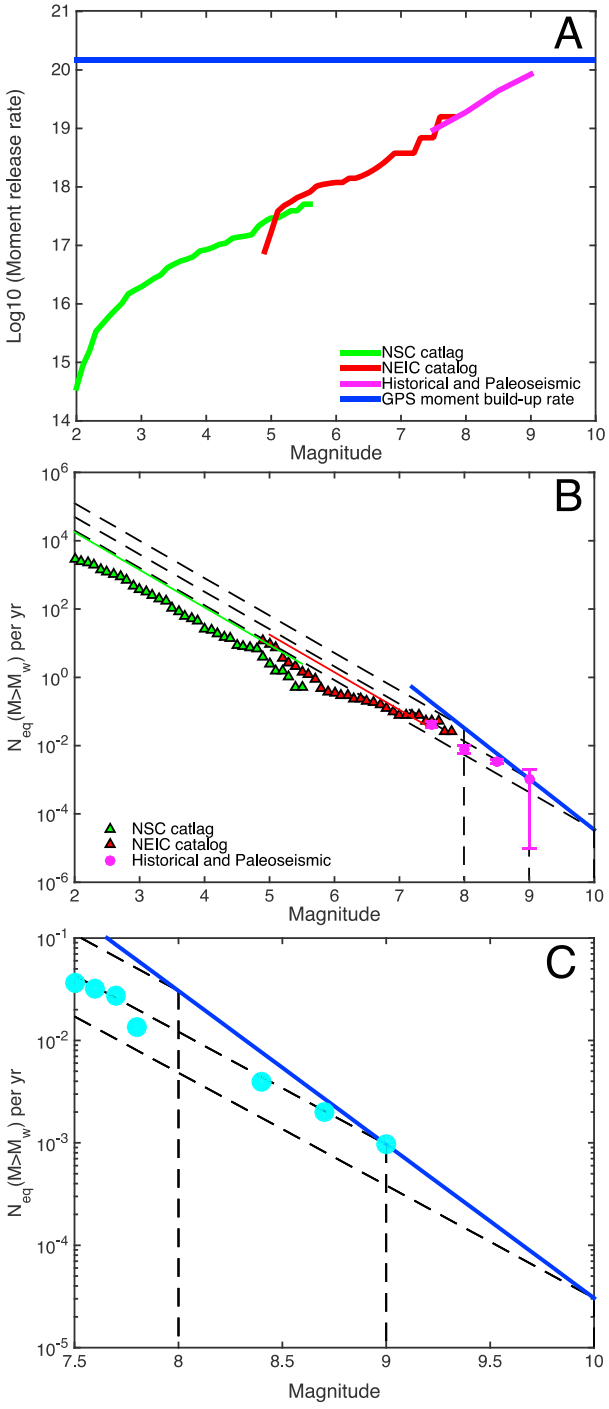

Figure 2.

Sunda Megathrust and the Longitudinal Valley fault in Taiwan. In these examples, the seismicity known from historical accounts and instrumental records and afterslip balance the interseismic deficit of moment [*Avouac*, 2015].

No spontaneous aseismic transient has yet been observed in the Himalaya despite nearly 20 years of monitoring with tectonic geodesy. Therefore, we deem the contribution of spontaneous transients small, though we cannot exclude the possibility of rare transients as observed on some subduction megathrust [*Radiguet et al.*, 2012; *Wallace and Beavan*, 2006]. More importantly, aseismic slip following large earthquakes, the so-called afterslip, could contribute significantly to the budget. Afterslip over the year following the M_w7.6, the 2005 Kashmir earthquake released possibly as much as $56 \pm 19\%$ of the coseismic moment [*Jouanne et al.*, 2011]. Afterslip in the first 2 months following the M_w7.8, the 2015 Gorkha earthquake released no more than 10% of the coseismic moment [*Galetzka et al.*, 2015].

Our calculations use the probability distribution function (pdf) of the rate of accumulation of the moment deficit in the interseismic period (Figure 1a, inset). Errors outside the formal errors in the seismic moment buildup rate are considered and would all lower the rate of buildup. First, if viscoelastic effects were significant, the elastic back slip model used would overestimate the buildup rate [*Wang et al.*, 2012; *Li et al.*, 2015], though since there have not been large earthquakes along the MHT recently, this effect is not likely to be significant. In Northern Chile, the viscoelastic effect was found to cause a bias of 12% (S. Li, personal communication, 2015), and while the tectonic setting is different here, we consider the bias to be $< 20\%$. The refined evaluation of this source of uncertainties is left to future studies. Second, unresolved creeping patches on the fault would also lower the buildup rate. However, to be unresolved, these patches would have to be small, and where we have the densest GPS we do not see any, suggesting there may be none at all. This suggests creeping patches could lower buildup rate by up to 10%.

From now on we assume that the moment released by seismic slip events is augmented by 50% due to a combination of aseismic afterslip and errors in seismic moment buildup rate, discussed above. Additionally, we first use the truncated Gutenberg-Richter (GR) law [e.g., *Working Group on California Earthquake Probabilities*, 1995; *Field et al.*, 1999] and then assume that the seismicity follows the (GR) law

up to the largest earthquake in the distribution (Method 1). Unlike other studies, we consider the effect of aftershocks produced by the larger earthquakes. If a very large earthquake has not occurred in the instrumental record (as is the case in the Himalaya, where the record is 39 years long), we will be missing all of its aftershocks. These would change the average rate of smaller earthquakes and shift the whole seismic curve upward. Excluding these aftershocks would lead to an overestimation in the maximum magnitude earthquake using the truncated GR method. Here we simulate missing aftershocks from the historical and paleoseismic earthquakes. We do this simply by using Bath's law for the largest aftershock (1.2 below the main shock) and then assuming that the smaller aftershocks follow a GR distribution with *b* value equal to the original earthquake catalog. The results of this can be seen in the green and red lines of Figure 2b.

For Method 1 we use Monte Carlo analysis and simulate 40 million different scenarios taking into account the uncertainties on the various quantities entering the calculation (the earthquake magnitude-frequency data themselves, the *b* value, the size of the largest aftershock, and the rate of moment accumulation). We extrapolate the frequency-magnitude relationship derived from the earthquake data sets to the magnitude needed to balance the slip budget (blue line in Figure 2b). We thus get the magnitude-frequency of the expected maximum earthquake.

Method 1 is incorrect if the frequency-magnitude GR distribution defined by the smaller earthquakes cannot be extrapolated to the largest event in the distribution, as is assumed in the characteristic earthquake model [*Schwartz and Coppersmith*, 1984]. It is indeed possible that the very large earthquakes, which rupture entirely the width of the seismogenic zone, do not follow the same statistics as the smaller events. We therefore make another calculation without this assumption (Method 2). We determine the 2-D pdf of the magnitude (M_w) and frequency ($1/T$, where T is the long-term-averaged return period) of the largest earthquake by multiplying the probability of balancing the slip budget, P1, and the probability of observing this largest earthquake over a given period of time, P2. P2 is calculated assuming that independent earthquakes follow a Poisson process and based on the largest known earthquake over the various periods of time covered by the earthquake catalogs. More details of the method and results obtained with different assumptions are given in the supporting information.

The data we analyze come from different earthquakes data sets as detailed in the supporting information. One is the seismicity of Nepal, which has been well monitored from a local network operated by the National Seismic Centre (NSC) Nepal [*Ader et al.*, 2012; *Pandey et al.*, 1999]. Another catalog is the 1976–2015 NEIC catalog which includes the M_w7.6 earthquake of 2005 and the M_w7.8 earthquake of 2015. The NEIC catalog yields a higher seismicity rate than the NSC catalog in the 4.5–5.5 magnitude range, where both catalogs are complete, due mostly to the contribution of the aftershocks of the 2005 and 2015 events. We next estimated the rate of $M_w > 7.5$, $M_w > 8.0$, $M_w > 8.5$, and $M_w > 9.0$ based on the historical catalog and take their aftershocks into account (Tables S1 and S2).

3. Results and Discussion

In Method 1 the data sets can be used independently or jointly to calculate the pdf of the magnitude and return period of the largest earthquake needed to close the slip budget, consistent with the GR law. Figure S2 shows that whatever catalog is used, the maximum earthquake would need to reach between M_w8.5 and M_w10. A M_w10 is unphysical, as a single rupture of the whole Himalayan arc (2500 km long),

Figure 2. Comparison of interseismic moment buildup and seismic moment released by known earthquakes. (a) Plot showing moment release rates for different sized earthquakes. Blue line shows the moment buildup rate calculated from the coupling pattern—the width of the line shows the errors. The curves showing the moment released by earthquakes are cumulative (all earthquakes with magnitude less than the abscissa value are added). The catalog of historical and paleoseismic events is listed in Table S1. The plot assumes one M_w9 event in the past 1000 years. With these assumptions, seismicity does not balance locking of the MHT in the interseismic period, and to do so, it would need to extend up to a magnitude more than M_w9. (b) Gutenberg-Richter plot with the same assumptions. The blue line shows the magnitude-recurrence time relationship of earthquakes that would take up the seismic moment. The black dashed lines show (top to bottom) where the seismicity should lie given an earthquake with maximum magnitude 8, 9, or 10, respectively, assuming that it follows the GR law with a *b* value of 1.1. The pink markers show the estimated long-term average seismicity rates and associated uncertainties (error bars show 1 sigma errors), by grouping magnitudes into bins of 0.5 magnitude unit range (Table S2). This allows for a better estimation of uncertainties. (c) Gutenberg-Richter plot of historical earthquakes (Table S1) compared with the frequency-magnitude of the largest event needed to balance the slip budget.

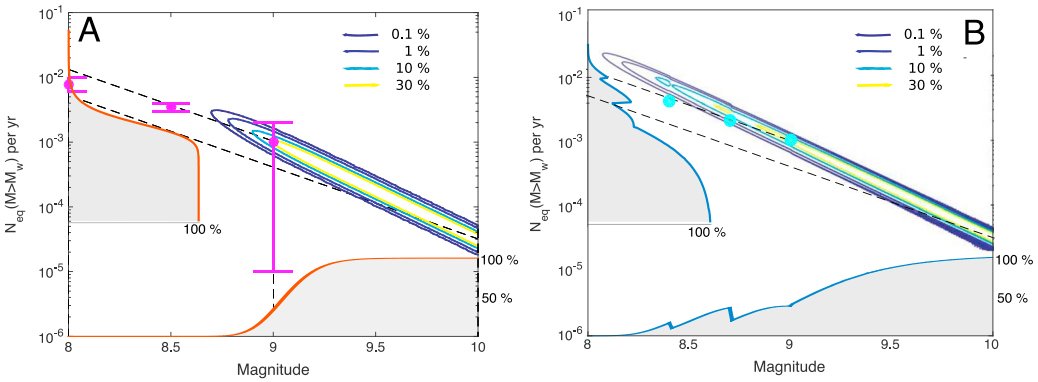

Figure 3. Probability distribution functions of the frequency-magnitude of the largest earthquake need to balance the slip budget. (a) Method 1. Colored contour lines show the 2-D pdf of the magnitude and frequency of the maximum earthquake. Grey shaded cumulative density functions along the *x* and *y* axes represent, respectively, the marginal cumulative probability of the largest earthquake exceeding a given magnitude, and the cumulative marginal probability of its frequency being lower than a given value. Pink markers show the binned magnitudes as in Figure 2b. (b) Method 2. As in Figure 3a, the shaded curves show the probability an earthquake of that magnitude, or recurrence time, could occur and take up the needed seismic moment. The probability drops after each of the magnitudes of the large earthquakes because above that magnitude, we have seen fewer earthquakes and they are short of balancing interseismic moment deficit. The drop after magnitude 9 is smaller because the recurrence time needed for a magnitude 9 to close the slip budget is closer to the observation period, 1000 years, so it is much more likely we could have missed an earthquake with this recurrence time. Blue markers showed the unbinned magnitudes, as in Figure 2c.

assuming a standard scaling law [*Schwartz and Coppersmith*, 1984] which implies an average slip of 50 m, would reach "only" M_w9.7. Figure 3a shows the 2-D pdf of the magnitude and frequency of the maximum earthquake (colored contour lines) as well as the marginal cumulative probability of the largest earthquake exceeding a given magnitude, and the cumulative marginal probability of its frequency being lower than a given value (grey shaded cumulative density functions along the *x* and *y* axis). The probability of closing the slip budget with the maximum event not exceeding M_w8.5 is extremely small (5.7×10^{-5}%). The probability of closing the slip budget with the largest earthquake not exceeding M_w9.0 is only about 34%. The probability of the return period of the largest event being more than 1000 years (corresponding to an annual frequency of less than 10^{-3}) is 66%. This analysis implies $M_w > 9$ events with a >1000 years return period at the 67% confidence level.

With Method 2, assuming earthquakes follow a Poisson distribution, the probability of closing the slip budget with the largest earthquake not exceeding M_w9.0 is about 37% (Figure 3b). The probability observing the largest event over 1000 years is now 45%. Both methods thus indicate that the largest earthquake in the Himalaya must exceed M_w9.0 at >63% confidence level. In both cases, the average return period of the largest earthquake is estimated to be >800 years at the whole arc scale.

Some studies have found suggestions of earthquake supercycles [e.g., *Sieh et al.*, 2008], though in the Himalaya we have not seen earthquake clustering in the past 500 years. To balance the moment with magnitude no larger than 8.5, we would need a magnitude 8.5 roughly once every 120 years. So, if only two occurred in the past 500 years, as the historical catalog suggests, this quiet period would need to be compensated by periods of clustered events, for example, a 500 year period with six events. We give this example although this possibility seems improbable to us in view of the paleoseismic data.

4. Conclusions

We conclude that millenary $M_w \geq 9.0$ earthquakes are very likely, confirming inference from paleoseismic studies [*Kumar et al.*, 2010; *Lavé et al.*, 2005; *Upreti et al.*, 2000]. To arrive at this result, we have used instrumental and historical/paleoseismic earthquake catalogs, along with the moment buildup rate derived from geodetic data. An alternative, less likely, scenario is that the rate of M_w8 to 8.5 earthquakes is much higher than estimated from historical data. In both cases, our analysis implies a high level of seismic hazard along most of the Himalayan arc.

Acknowledgments
This work was supported by NSF grant 1345136. The earthquake catalog data can be found on the websites indicating within the text and within the supporting information.

References

Ader, T., et al. (2012), Convergence rate across the Nepal Himalaya and interseismic coupling on the Main Himalayan Thrust: Implications for seismic hazard, *J. Geophys. Res.*, *117*, B04403, doi:10.1029/2011JB009071.

Avouac, J. P. (2003), Mountain building, erosion and the seismic cycle in the Nepal Himalaya, in *Advances in Geophysics*, edited by R. Dmowska, pp. 1–79, Elsevier, Amsterdam.

Avouac, J.-P. (2015), From geodetic imaging of seismic and aseismic fault slip to dynamic modeling of the seismic cycle, *Annu. Rev. Earth Planet. Sci.*, *43*(43), 233–271.

Berthet, T., J.-F. Ritz, M. Ferry, P. Pelgay, R. Cattin, D. Drukpa, R. Braucher, and G. Hetenyi (2014), Active tectonics of the eastern Himalaya: New constraints from the first tectonic geomorphology study in southern Bhutan, *Geology*, *42*(5), 427–430.

Bilham, R., et al. (1997), GPS measurements of present-day convergence across the Nepal Himalaya, *Nature*, *386*(6620), 61–64.

Bilham, R., V. K. Gaur, and P. Molnar (2001), Earthquakes: Himalayan seismic hazard, *Science*, *293*(5534), 1442–1444.

Bollinger, L., J. P. Avouac, R. Cattin, and M. R. Pandey (2004), Stress buildup in the Himalaya, *J. Geophys. Res.*, *109*, B11405, doi:10.1029/2003JB002911.

Bollinger, L., S. N. Sapkota, P. Tapponnier, Y. Klinger, M. Rizza, J. Van der Woerd, D. R. Tiwari, R. Pandey, A. Bitri, and S. B. de Berc (2014), Estimating the return times of great Himalayan earthquakes in eastern Nepal: Evidence from the Patu and Bardibas strands of the Main Frontal Thrust, *J. Geophys. Res. Solid Earth*, *119*, 7123–7163, doi:10.1002/2014JB010970.

Brune, J. N. (1968), Seismic moment seismicity and rate of slip along major fault zones, *J. Geophys. Res.*, *73*(2), 777–784, doi:10.1029/JB073i002p00777.

Field, H., D. D. Jackson, and J. F. Dolan (1999), A mutually consistent seismic-hazard source model for Southern California, *Bull. Seismol. Soc. Am.*, *89*(3), 559–578.

Galetzka, J., et al. (2015), Slip pulse and resonance of Kathmandu basin during the 2015 M_w 7.8 Gorkha earthquake, Nepal imaged with geodesy, *Science*, *349*(6252), 1091–1095, doi:10.1126/science.aac6383.

Jouanne, F., A. Awan, A. Madji, A. Pecher, M. Latif, A. Kausar, J. L. Mugnier, I. Khan, and N. A. Khan (2011), Postseismic deformation in Pakistan after the 8 October 2005 earthquake: Evidence of afterslip along a flat north of the Balakot-Bagh thrust, *J. Geophys. Res.*, *116*, B07401, doi:10.1029/2010JB007903.

Kumar, S., S. G. Wesnousky, T. K. Rockwell, R. Briggs, V. C. Thakur, and R. Jayangondaperumal (2006), Paleoseismic evidence of great surface-rupture earthquakes along the Indian Himalaya, *J. Geophys. Res.*, *111*, B03304, doi:10.1029/2004JB003309.

Kumar, S., S. G. Wesnousky, R. Jayangondaperumal, T. Nakata, Y. Kumahara, and V. Singh (2010), Paleoseismological evidence of surface faulting along the northeastern Himalayan front, India: Timing, size, and spatial extent of great earthquakes, *J. Geophys. Res.*, *115*, B12422, doi:10.1029/2009JB006789.

Lavé, J., D. Yule, S. Sapkota, K. Basant, C. Madden, M. Attal, and R. Pandey (2005), Evidence for a great medieval earthquake (approximate to 1100 AD) in the Central Himalayas, Nepal, *Science*, *307*(5713), 1302–1305.

Li, S., M. Moreno, J. Bedford, M. Rosenau, and O. Oncken (2015), Revisiting viscoelastic effects on interseismic deformation and locking degree: A case study of the Peru-North Chile subduction zone, *J. Geophys. Res. Solid Earth*, *120*, 4522–4538, doi:10.1002/2015JB011903.

Molnar, P. (1979), Earthquake recurrence intervals and plate tectonics, *Bull. Seismol. Soc. Am.*, *69*(1), 115–133.

Mukul, M., S. Jade, A. K. Bhattacharyya, and K. Bhusan (2010), Crustal shortening in convergent orogens: Insights from Global Positioning System (GPS) measurements in northeast India, *J. Geol. Soc. India*, *75*(1), 302–312.

Pandey, M. R., R. P. Tandukar, J.-P. Avouac, J. Vergne, and T. Héritier (1999), Seismotectonics of Nepal Himalayas from a local seismic network, *J. Asian Earth Sci.*, *17*, 703–712.

Radiguet, M., F. Cotton, M. Vergnolle, M. Campillo, A. Walpersdorf, N. Cotte, and V. Kostoglodov (2012), Slow slip events and strain accumulation in the Guerrero gap, Mexico, *J. Geophys. Res.*, *117*, B04305, doi:10.1029/2011JB008801.

Schiffman, C., B. S. Bali, W. Szeliga, and R. Bilham (2013), Seismic slip deficit in the Kashmir Himalaya from GPS observations, *Geophys. Res. Lett.*, *40*, 5642–5645, doi:10.1002/2013GL057700.

Schwartz, D. P., and K. J. Coppersmith (1984), Fault behavior and characteristic earthquakes: Examples from the Wasatch and San Andreas fault zones, *J. Geophys. Res.*, *89*, 5681–5698, doi:10.1029/JB089iB07p05681.

Sieh, K., D. H. Natawidiaia, A. J. Meltzner, C. C. Shen, H. Cheng, K. S. Li, B. W. Suwargadi, J. Galetzka, B. Philibosian, and R. L. Edwards (2008), Earthquake supercycles inferred from sea-level changes recorded in the corals of West Sumatra, *Science*, *322*(5908), 1674–1678.

Stevens, V. L., and J. P. Avouac (2015), Interseismic coupling on the main Himalayan thrust, *Geophys. Res. Lett.*, *42*, 5828–5837, doi:10.1002/2015GL064845.

Styron, R. H., M. H. Taylor, and M. A. Murphy (2011), Oblique convergence, arc-parallel extension, and the role of strike-slip faulting in the High Himalaya, *Geosphere*, *7*(2), 582–596.

Upreti, B. N., T. Nakata, Y. Kumahara, H. Yagi, K. Okumura, T. K. Rockwell, N. S. Verdi, and H. Maemoku (2000), The latest active faulting in southeast Nepal: In active fault research for the new millenium, in *Proceedings of the Hokudan International Symposium and School on Active Faulting*, edited by K. T. K. Okumura and H. Goto, pp. 533–536, Letter Press Ltd., Hiroshima, Japan.

Wallace, L. M., and J. Beavan (2006), A large slow slip event on the central Hikurangi subduction interface beneath the Manawatu region, North Island, New Zealand, *Geophys. Res. Lett.*, *33*, L11301, doi:10.1029/2006GL026009.

Wang, K., Y. Hu, and J. He (2012), Deformation cycles of subduction earthquakes in a viscoelastic Earth, *Nature*, *484*, 327–332.

Working Group on California Earthquake Probabilities (1995), Seismic hazards in southern California: Probable earthquakes, 1994 to 2024, *Bull Seismol. Soc. Am.*, *85*, 379–439.